HHS Public Access

Author manuscript

Mater Des. Author manuscript; available in PMC 2019 July 15.

Published in final edited form as:

Mater Des. 2018 July 15; 150: 182–187. doi:10.1016/j.matdes.2018.04.013.

Inkjet Printed Polyethylene Glycol as a Fugitive Ink for the Fabrication of Flexible Microfluidic Systems

Ahmed Alfadhel[1,+], **Jing Ouyang**[1,+], **Chaitanya G. Mahajan**[2], **Farzad Forouzandeh**[1], **Denis Cormier**[2], and **David A. Borkholder**[1,*]

[1]Microsystems Engineering, Rochester Institute of Technology, Rochester, NY 14623, USA

[2]Industrial and Systems Engineering, Rochester Institute of Technology, Rochester, NY 14623, USA

Abstract

This paper demonstrates a novel and simple processing technique for the realization of scalable and flexible microfluidic microsystems by inkjet-printing polyethylene-glycol (PEG) as a sacrificial template, followed by embedding in a structural layer (e.g. soft elastomers). The printing technology allows production of an array of PEG droplets simultaneously, reducing cost and manufacturing time. The PEG can be removed through heating above its phase-change temperature after the formation of the structural layer, with hydraulic flow removing the material. The developed technique allows easy modulation of the shape and dimensions of the pattern with the ability to generate complex architectures without using lithography. The method produces robust planar and multilayer microfluidic structures that can be realized on wide range of substrates. Moreover, microfluidics can be realized on other systems (e.g. electrodes and transducers) directly without requiring any bonding or assembling steps, which often limit the materials selection in conventional microfluidic fabrication. Multilayer Polydimethylsiloxane (PDMS) microfluidic channels were created using this technique to demonstrate the capability of the concept to realize flexible microfluidic electronics, drug delivery systems, and lab-on-a-chip devices. By utilizing conductive liquid metals (i.e. EGaIn) as the filling material of the channels, flexible passive resistive components and sensors have been realized.

Graphical abstract

*Corresponding author (david.borkholder@rit.edu).
+Contributed equally to the manuscript

DATA AVAILABILITY

The raw/processed data required to reproduce these findings cannot be shared at this time due to technical or time limitations.

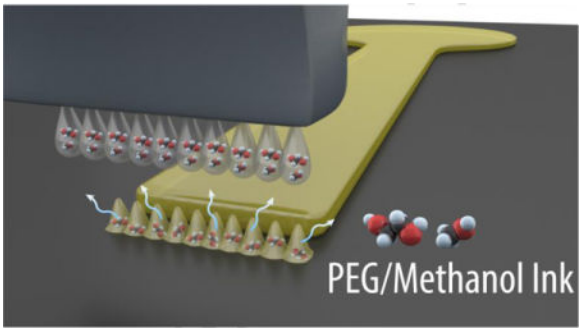

Keywords

inkjet printing; polyethylene glycol; microfluidic; microsystems; flexible electronics

1. Introduction

The requirement of compact and integrated systems promotes the development of flexible microfluidic devices in recent decades. Several applications have been demonstrated using microfluidics technology including drug delivery systems [1], biosensing [2] and lab-on-chip applications [3]. Flexible electronics have also been developed using microfluidics technology to realize applications such as passive electronics, energy harvesters, bio-inspired devices, and wearable healthcare sensors [4–7]. Microfluidic systems have been realized using conventional microfluidic fabrication techniques. However, fabrication challenges and material incompatibilities pose barriers to achieving the full potential of this emerging field, and limit device capabilities and scalability [8]. Conventional microfluidic channel fabrication requires patterning a mold for soft polymeric structural layer replication. Several methods have been reported to pattern the mold such as lithography techniques [9], or etching based methods [10, 11]. A replica is then created by depositing the structural layer on the mold that contains the patterned features to define the channels. PDMS is a common polymeric structural layer for microfluidics due to its biocompatibility, transparency, chemical resistance, easy realization and shape modulation [12, 13]. The patterned structural layer can then be peeled off and bonded to the target substrate (e.g. silicon, PDMS or glass). However, selection of the substrate material is limited due to the bonding quality between the structural material and the substrate. Moreover, the peeling-off step may damage the structural layer or the microfluidic features, which can negatively affect microfluidic system performance. The bonding process typically requires surface modification, thermal processing, and applying pressure to ensure full contact in addition to precise alignment. Moreover, most existing techniques are planar, creating barriers to realization of multilayer 3D channels required for applications such as replication of complex microvasculature [14, 15], or for high density microfluidic networks in space constrained applications [16].

To avoid the issues associated with conventional molding, peeling-off, and bonding processes, and to expand the range of structural and substrate materials, techniques such as direct 3D printing of the microfluidic channels [17] and sacrificial molding [18] have been investigated. Layer-by-layer 3D printing of channels can achieve good resolution and allows

the realization of complex geometries. However, 3D printing has limited materials selection and does not allow channels to be directly created on any substrate independent of specific support material requirements. These limit the realization of flexible microfluidics or the direct integration of microfluidics on other systems.

Direct patterning of a sacrificial layer that is subsequently encapsulated by a polymer is an emerging approach for fabricating microchannels. The sacrificial layer can then be removed using a stimulus such as heat to melt [19] or evaporate [20] the layer and clear the channels. Other techniques include layer dissolution [18], and chemical etching [21]. Fabricating sacrificial layers using additive manufacturing techniques has been a novel approach that allows rapid fabrication of structures with reduced cost and complexity. Different types of 'fugitive' inks have been 3D printed such as EGaIn liquid metal, a eutectic alloy of gallium (Ga) and indium (In) [22]. This approach allows realizing multilayer microfluidic channels, however, removing this ink requires chemicals that are not biocompatible [22], and the large circular cross-section of the printed EGaIn prevents fine resolution or full control over channel dimensions. Several other fugitive inks have been printed; however, they usually need harsh chemicals or require long dissolution time to remove the ink. A promising technique has been reported based on 3D printing of a water-soluble sugar alcohol isomalt to form a sacrificial layer that can be simply removed by dipping in water after encapsulation in a structural layer, leaving behind a hollow microfluidic channel [18]. This technique is limited in dimensions with minimum resolution of 250 μm and provides fixed circular channel cross-section, which is difficult to realize on any substrate. Consequently, there is a demand to have a new sacrificial material to address these aforementioned limitations.

Phase change materials have been introduced for sacrificial molding due to their high removability when heated above their phase change temperature without leaving any residue to contaminate the microfluidic system. Wax [23] and hydrogels [24] have been demonstrated for applications in microfluidics. Polyethylene Glycol (PEG) in particular has attracted interest for sacrificial molding due to its biocompatibility [25] and the phase change property at modestly elevated temperatures. PEG has been patterned previously using several approaches such as molding [26], pattern transfer [27], and atomic force microscopy based dip-pen nanolithography [28]. As an alternative to these conventional approaches for PEG patterning, the use of inkjet printing offers a high resolution and Computer-aided design (CAD) driven maskless process, which allows fabricating microscale structures. Inkjet-printing is an additive manufacturing technique that uses liquid phase droplets ejection from the nozzle featuring no material waste. Compared to other printing techniques, inkjet printing allows much smaller printable layer thickness leading to a better vertical resolution in addition to short printing duration.

In this paper, we introduce the printing and characterization of PEG as a sacrificial layer for microfluidics. This process relies on a unique multi-nozzle inkjet printing technology that enables rapid fabrication of microfluidic channels on a wide range of substrates. This not only significantly simplifies the microfluidic system fabrication, but also creates the possibility to realize microfluidic systems and electronics for a wide range of applications.

Flexible electronic have gained significant attention for their wide range of applications such as epidermal electronics for human health monitoring [29, 30] due to the enhanced performance from their high deformability and conformal contact, in addition to their lightweight and low cost [30]. A limitation in current flexible and stretchable electronics is the incorporation of rigid components and sensing elements that are bonded to the substrate [31]. These challenges hinder the ultimate utility of flexible electronics. An emerging approach for flexible electronics is the realization of deformable and shape-reconfigurable all-soft microfluidic-based electronics with the use of liquid-phase conductors [32]. Among possible conductive liquids, EGaIn is of an interest because of its excellent mechanical properties, high electrical conductivity, low melting temperature, and low toxicity [22, 32]. Resistive microfluidic electronics are fabricated in this paper as a proof-of-concept and demonstration for the capabilities of the developed technology.

2. Materials and Methods

2.1 Ink Preparation

The fugitive ink was made out of PEG with molecular weight of 2000 (50–53°C melting temperature) and dissolved in Methanol with 1:1 ratio. Methanol was used to maintain the PEG in a liquid state for inkjet printing while keeping the surface tension below 30 dyne/cm such that the ejected droplets can overcome the capillary force to avoid retraction back into the nozzle of the inkjet printer [33]. Surface tension of the prepared PEG ink was measured by a tensiometer (Model 250, Rame-Hart) and was found to be 22.32 dyne/cm, which is in the printable range.

2.2 PEG Printing

The prepared ink was transferred to a 16-nozzle cartridge with 10 pL printed drop volume and installed on the Inkjet printer (Fuji Dimatix, DMP-3000). The printing head moves in the X direction while the substrate is mounted on a stage that moves in the Y and Z direction. It is important to optimize the printing parameters (i.e. drop spacing and dispensing voltage), as well as the substrate property to be able to form continuous lines and defined features while simultaneously obtaining high resolution to expand the size range of the printable features. Understanding the ejected droplet behavior once it gets in contact with the substrate is the key step that allows optimizing the printing parameters. The droplet's contact angle has an influence on the droplet drying patterns, and hence an influence on the targeted features and the final line width, with higher contact angle substrates leading to narrower lines [34]. However, lines printed on a low surface energy substrate (high contact angle; >90°) can easily form bulging or discontinuity caused by the build-up of internal pressure during evaporation of methanol [35]. If the surface is hydrophilic and the printed droplets have low contact angle (i.e. <90°), the droplet will tend to stay spread during the evaporation of Methanol which allows having the droplets merged together and form continuous lines. Tuning the printed droplet spacing as well as the substrate surface energy is necessary to obtain uniform lines and improve the resolution. In this work, contact angle measurements were conducted using a Tensiometer (Rame-Hart, 250), and surface energy was modified using an Oxygen plasma (Harrick Plasma, PDC-32G). The structure and

dimensions of the printed PEG droplets and features were measured using an optical microscope and optical profilometer (Nanovea, ST400).

2.3 Microfluidic Channel Fabrication

The developed fabrication process of microfluidic channels involves three main steps, as shown in Fig. 1. In the first step, an inkjet printer deposits a sacrificial layer in the desired channel geometry on a substrate (e.g. PDMS), which becomes the base of the microchannel. The width of the channel is defined by the number of droplet rows (i.e. each droplet row is considered a pixel), and the utilized approach allows printing 16 pixels simultaneously with a full control on the droplet spacing and ejection specifications. The channel thickness can be controlled by the number of printed layers with great consistency. After printing the sacrificial layer, which solidifies upon landing on the substrate due to the evaporation of Methanol, the channel's structural layer is deposited which can be done using different materials. In this work, PDMS (Dow Corning, Sylgard 184) with 10:1 elastomer base to cross-linker ratio is deposited by a drop-casting method to form the structural layer. PDMS is then cured at 45 °C for 10 hours to ensure that the PDMS is fully cured without melting the sacrificial layer. After that, the openings (inlet and outlet) of the microfluidic channel were realized using a 1 mm diameter biopsy punch and tubing (1/16" OD, 1/32" ID) was connected in the inlet and the outlet to form the continuous microfluidic path. The PEG sacrificial layer can be removed through heating above its phase-change temperature and dissolving in solutions such as Isopropyl alcohol (IPA), water and Methanol. The PEG structure is heated on a hot plate at 60 °C for 10 minutes to ensure full melting, and then heated IPA is injected using a syringe pump (New Era, NE-1000) to wash away PEG while keeping the structure heated. The channel is then ready to use with injecting the required fluid.

The presented process can be utilized to fabricate multilayer microfluidic structures with a level-by-level mechanism. Every channel layer is defined as a new level that utilizes the underlying structural layer as a substrate, and repeats the sacrificial layer printing and structural layer deposition. Each level is independent in terms of fabrication, enabling a broad range of channel shape and dimensions (i.e. length, width and thickness), structural material combinations, and sensor integration (e.g. electrodes). Interconnecting the multilayer channels is also possible by introducing the interconnection ports in the PDMS structural layer using a biopsy punch, and printing PEG plugs to fill the port prior to printing the upper channel sacrificial layer. Other techniques can be utilized for easier multilayer fabrication if the structural layer is printed instead of the demonstrated casting process.

2.4 Microfluidic Electronics

To demonstrate microfluidic electronics, fabricated channels were filled with EGaIn liquid metal to act as an all-soft passive resistive component. EGaIn is of an interest due to its excellent electrical and mechanical properties, including high electrical conductivity (σ = 3.4×10^6 S m^{-1}), and low toxicity [22, 32]. In addition, EGaIn is a liquid under ambient conditions with a melting point of 15.5 °C with a thin passivating oxide shell formed instantaneously on the surface of the metal at room temperature in the presence of oxygen [36]. This provides the opportunity to form stable and conductively functional flexible

devices that are shape-reconfigurable in response to bending or twisting. Since the oxide shell is expected to prevent efficient filling of the microfluidic channel, the liquid metal is washed with 1 M Hydrochloric acid to remove the oxide shell prior to injecting it in the channel. A SourceMeter (Keithley, 2636A) is used to measure the electrical properties of the realized devices.

To estimate the change in the resistance due to bending or applying pressure, finite element simulations were conducted in COMSOL multiphysics® utilizing Solid Mechanics and Electric Current physics, with 2D axisymmetric geometry. The application of these two physics modules enabled simplification of the EGaIn sensor into a linear elastic material, with estimated changes in the resistance under deformation equivalent to the experimental system. The dimensions and material properties were assigned according to the actual fabricated devices with Poisson's ratio of 0.47 and Young's modulus of 450 kPa.

3. Results and Discussion

PEG inkjet printing was optimized on PDMS substrates with emphasis on resolution and feature definition. The diameter of ejected PEG droplets changes as they land on the substrate and the methanol evaporates, with the final diameter heavily dependent on the surface energy of the substrate. By controlling this surface energy through oxygen plasma treatment, the substrate can be modified to make it more hydrophilic with lower contact angle. Efficient printing with optimized resolution and feature definition was achieved with a surface contact angle of 60°. These parameters were utilized throughout the studies in this paper. The PEG droplet size as printed on the substrate was measured at 50 μm as shown in the microscope image of Fig. 2(a). Tuning the drop spacing allows continuous lines with good uniformity to be realized, with an optimal center-to-center drop spacing of 30 μm yielding single pixel width lines 50 μm wide and 2.5 μm thick (Fig. 2(b)) with a semicircular cross-section profile. Multi-pixel lines are achieved with a 30 μm y-direction shift between each printed line, resulting in partial overlap and line width increases as shown in the measured profiles of Fig. 2(c). Since printing occurs in the liquid state of PEG and droplets merge and overlap, the thickness of the printed feature increases with wider printed features. Multiple PEG layers can be printed consecutively without y-direction shifts to linearly increase the thickness as shown in Fig. 2(d). It is also observed that the width increases slightly when printing multiple layers due to the flowing of liquid PEG prior to solidification.

PDMS Microfluidic channels were fabricated to demonstrate the potential of realizing microfluidic applications. A CAD drawing is used to define the PEG horizontal pattern that is then decomposed into a grid of pixels by the inkjet printer and realized by a drop matrix with a fixed drop spacing (i.e. 30 μm in this work). The height of the patterns is defined by the number of pixels and the number of printed layers. These parameters are critical to define the minimal resolution. The PDMS channels were realized by printing 5 layers of 100 μm wide PEG with a 4 mm diameter center chamber on a 1 mm thick PDMS substrate as shown in Fig. 3(a), followed by the casting of uncured PDMS to form the structural layer. After curing PDMS and realizing the inlet and outlet, PEG is heated above its phase change temperature and washed away, leaving a hollow PDMS channel with the same shape and

dimensions as the printed PEG pattern. The flexible channel can then be filled with the required fluid as shown in Fig. 3(b). The same process is used to realize multilayer microfluidic channels by printing a second sacrificial layer on the first structural layer, followed by a second structural layer fabrication. As an example of such geometries, overlapped 1 mm and 0.5 mm wide channels were fabricated as shown in Fig. 3(c).

EGaIn-based, flexible electronic passive components (i.e. resistors) were fabricated to demonstrate the capability of the reported technology as shown in Fig. 4. The resistance can be designed based on the channel dimensions. Because EGaIn is liquid, the shape of a microchannel filled with EGaIn can be changed in response to bending or twisting, making it shape-reconfigurable, which leads to a change in the resistance. A 2 cm long, 100 μm wide and 3 μm thick PDMS microfluidic channel was fabricated using the PEG inkjet printing process, and then filled with EGaIn to form a resistive line. Cu pads were connected at the sides of the resistor to form electrical contacts. The resistance $R=\rho L/A$ was estimated by the resistivity ρ of EGaIn (29.4×10^{-8} Ω-m) as well as the cross-sectional area A (1.86×10^{-10} m^2) obtained from the 3-pixel profile in Fig. 2(c), and the channel length L (0.02 m), which was found to be 31.6 Ω. The DC electrical characteristics of the resistor were investigated by obtaining the $I–V$ curve for the conductor line, where resistance was found to be 36 Ω. This is slightly higher than the estimation (i.e. 31.6 Ω) due to slight variation in the cross-sectional area along the length of the channel, in addition to possible experimental error when calibrating the measurement setup. An important feature of the microfluidic resistor is its stretchability, where the continuous conductive path is maintained while stretching as shown in Fig. 4(a), with an increase in the resistance as the cross section of the channel narrows with stretching. The resistor is also foldable and can be bent while maintaining electrical conductivity. The change in relative resistance $\Delta R/R_0$ was investigated as shown in Fig. 4(c) and compared to the simulated results, where ΔR is the difference in resistance before and after bending, and R_0 is the initial resistance. The resistor is bent along the length direction and the resistance is obtained at different radii of curvature. As the radius of curvature becomes smaller, the relative resistance gradually increases to 8% for a radius of curvature of 15 mm, representing bending on the thumb. This increase in resistance upon bending can be explained by the change in geometry where bending along the length direction increases the resistor length and decreases the microfluidic resistor cross-sectional area. The simulated response exhibits a similar behavior to the experimental results over a range of bending radii, with the change in curvature driving geometric changes and associated sensor resistance shifts. This influence is most substantial in smaller curvature radii resulting in significant change of resistance. Some deviation is obtained in the simulated response at high curvatures, which is likely due to simplifications in the numerical model where linear elastic properties are considered, while hyperelastic behavior under large strain is neglected. These results indicate the suitability of such resistors for strain sensing with the flexibility to optimize the shape and resistance to target specific applications and obtain specific sensitivity and operating range.

Liquid metal microfluidic passive resistors can also be utilized for pressure or tactile sensing as reported previously using the conventional microfluidic fabrication processes [32]. A more efficient and flexible approach can be utilized with the PEG inkjet printing process to realize microfluidic sensors with wide range of materials and on different substrates. The

design of the pressure sensor in this work consists of a central circular area with a diameter of 8 mm and height of 32 μm, in addition to 5 mm long and 200 μm wide channels in the sides as shown in Fig. 5. The top PDMS structural layer, which defines the membrane in the active area, is 1 mm thick and has a Young's modulus of 450 kPa. When a load is applied to the pressure-sensing region, the membrane bends causing the fluid to be displaced to the side regions, changing the cross-sectional area and affecting the overall resistance of the sensor. When the load is removed, the fluid is pushed back to the circular sensing region and the resistance returns to its initial value. The relative resistance $\Delta R/R_0 \tilde{} P/E_c$ is proportional to the applied load P and the compressive modulus E_c of the deformable PDMS membrane [32]. Moreover, the diameter of the sensor region defines the loading capacity of the pressure sensor. By considering these parameters, a localized pressure sensor can be obtained with tailored sensitivity and operating range. The developed pressure sensor is characterized by applying static loads up to 35 kPa and measuring the change in relative resistance. A linear response is observed up to 25 kPa with a sensitivity of 0.24 kPa^{-1}. Beyond this pressure, the PDMS is tightly compressed and the response begins to saturate. Fig. 5 shows the response of the fabricated sensor under applied pressures, and compared to the response of the simulated device. The measured changes in the resistances agreed well with the numerical results at pressures lower than 25 kPa. The main source for the deviation at higher pressures can be attributed to the model simplifications described above. The results in general demonstrate a great potential for such highly customizable pressure sensors to be used as a microfluidic wearable technology for wide range of applications.

4. Conclusion

In conclusion, this paper demonstrates a unique method for fabricating microfluidic systems based on PEG as a fugitive ink, patterned via an inkjet printing direct-write approach. The printing technology enables robust planar and multilayer microfluidic structures to be realized, with easy modulation of the shape and dimensions and with high vertical resolution. This technique creates the opportunity of simplifying the fabrication of microfluidic structures, and opens the door to achieving scalable and flexible microfluidic systems on a broad range of substrates. The ability to fabricate multilayer microfluidic channels as well as passive flexible microfluidic electronics is demonstrated on PDMS substrates and with utilizing conductive liquid metals. This research opens an opportunity to realize highly customizable wearable microfluidic devices for wide range of applications.

Acknowledgments

This research was partially supported by the National Institute on Deafness and Other Communication Disorders – NIDCD, of the National Institutes of Health under Grant Award Number R01 DC014568.

References

1. Johnson D, Waldron M, Frisina R, Borkholder D. Implantable micropump technologies for murine intracochlear infusions, 2010. Annual International Conference of the IEEE Engineering in Medicine and Biology. 2010
2. Medina-Sánchez M, Miserere S, Morales-Narváez E, Merkoçi A. On-chip magneto-immunoassay for Alzheimer's biomarker electrochemical detection by using quantum dots as labels. Biosensors and Bioelectronics. 2014; 54:279–284. [PubMed: 24287417]

3. Dittrich PS, Manz A. Lab-on-a-chip: microfluidics in drug discovery. Nat Rev Drug Disc. 2006; 5:210–218.
4. Yeo JC, Kenry, Lim CT. Emergence of microfluidic wearable technologies. Lab Chip. 2016; 16:4082–4090. [PubMed: 27713996]
5. Cheng S, Wu Z. Microfluidic electronics. Lab Chip. 2012; 12:2782–2791. [PubMed: 22711057]
6. Takei K, Takahashi T, Ho JC, Ko H, Gillies AG, Leu PW, Fearing RS, Javey A. Nanowire active-matrix circuitry for low-voltage macroscale artificial skin. Nature Materials. 2010; 9:821. [PubMed: 20835235]
7. Yeo WH, Kim YS, Lee J, Ameen A, Shi L, Li M, Wang S, Ma R, Jin SH, Kang Z, Huang Y, Rogers JA. Multifunctional epidermal electronics printed directly onto the skin. Advanced Materials. 2013; 25:2773. [PubMed: 23440975]
8. Go JS, Shoji S. A disposable, dead volume-free and leak-free in-plane PDMS, microvalve, Sensors and Actuators. A: Physical. 2004; 114:438–444.
9. Tang SK, Whitesides GM. Basic microfluidic and soft lithographic techniques, Optofluidics Fundam. In: Fainman Y, Lee L, Psaltis D, Yang C, editorsDevices Appl. McGraw-Hill; 2010.
10. Gattass RR, Mazur E. Femtosecond laser micromachining in transparent materials. Nature Photonics. 2008; 2:219–225.
11. Roberts MA, Rossier JS, Bercier P, Girault H. UV Laser Machined Polymer Substrates for the Development of Microdiagnostic Systems. Anal Chem. 1997; 69:2035–2042. [PubMed: 21639243]
12. Lee JN, Park C, Whitesides GM. Solvent Compatibility of Poly(dimethylsiloxane)-Based Microfluidic Devices. Anal Chemistry. 2003; 75:6544–6554.
13. Belanger MC, Marois Y. Hemocompatibility, Biocompatibility, inflammatory and in vivo studies of primary reference materials low-density polyethylene and polydimethylsiloxane: a review. Journal of Biomedical Materials Research. 2001; 58:467–77. [PubMed: 11505420]
14. Olugebefola SC, et al. Polymer microvascular network composites. Journal Compos Mater. 2010; 44:2587–2603.
15. Therriault, White SR, Lewis JA. Chaotic mixing in three-dimensional microvascular networks fabricated by direct-write assembly. Nature Materials. 2003; 2:265–271. [PubMed: 12690401]
16. Meyvantsson I, Warrick JW, Hayes S, Skoienb A, Beebe DJ. Automated cell culture in high density tubeless microfluidic device arrays. Lab Chip. 2008; 8:717–724. [PubMed: 18432341]
17. Erkal JL, Selimovic A, Gross BC, Lockwood SY, Walton EL, McNamara S, Spence DM. 3D Printed Microfluidic Devices with Integrated Versatile and Reusable Electrodes. Lab Chip. 2014; 14:2023–2032. [PubMed: 24763966]
18. Gelber MK, Bhargava R. Monolithic multilayer microfluidics via sacrificial molding of 3D-printed isomalt. Lab Chip. 2015; 15:1736–1741. [PubMed: 25671493]
19. Toohey KS, Sottos NR, Lewis JA, Moore JS, White SR. Self-healing materials with microvascular networks. Nature Materials. 2007; 6:581–585. [PubMed: 17558429]
20. Nguyen DT, Leho YT, Esser-Kahn AP. A threedimensional microvascular gas exchange unit for carbon dioxide capture. Lab Chip. 2012; 12:1246–1250. [PubMed: 22344348]
21. Zhang H, Yu X, Braun PV. Three-dimensional bicontinuous ultrafast-charge and -discharge bulk battery electrodes. Nature Nanotechnology. 2011; 6:277–281.
22. Parekh DP, Ladd C, Panich L, Moussa K, Dickey MD. 3D printing of liquid metals as fugitive inks for fabrication of 3D microfluidic channels. Lab Chip. 2016; 16:1812–1820. [PubMed: 27025537]
23. Dharmatilleke S, Henderson HT, Bhansali S, Ahn CH. Three-dimensional silicone microfluidic interconnection scheme using sacrificial wax filaments. Proceedings of SPIE Microfluidic devices and systems III. 2000; 4177:83–90.
24. Lee W, et al. On-Demand Three-Dimensional Freeform Fabrication of Multi-Layered Hydrogel Scaffold With Fluidic Channels, Biotechnol. Bioeng. 2010; 105:1178–1186.
25. Alcantar N, Aydil E, Israelachvili J. Polyethylene glycol-coated biocompatible surfaces. Journal of Biomedical Materials Research. 2000; 51:343–351. [PubMed: 10880075]
26. Suh KY, Langer R. Microstructures of poly (ethylene glycol) by molding and dewetting. Applied Physics Letter. 2003; 38:1668–2003.

27. Acton Q. Polyethylene Glycols—Advances in Research and Application: 2013 Edition. Scholarly Editions. 2013:384.
28. Sanedrin RG, Huang L, Jang JW, Kakkassery J, Mirkin CA. Polyethylene Glycol as a Novel Resist and Sacrificial Material for Generating Positive and Negative Nanostructures. Small. 2008; 4:920–924. [PubMed: 18563746]
29. Takei K, Takahashi T, Ho JC, Ko H, Gillies AG, Leu PW, Fearing RS, Javey A. Nanowire active-matrix circuitry for low-voltage macroscale artificial skin. Nature Materials. 2010; 9:821. [PubMed: 20835235]
30. Yeo WH, Kim YS, Lee J, Ameen A, Shi L, Li M, Wang S, Ma R, Jin SH, Kang Z, Huang Y, Rogers JA. Multifunctional epidermal electronics printed directly onto the skin. Advanced Materials. 2013; 25:2773. [PubMed: 23440975]
31. Xu S, Zhang Y, Jia L, Mathewson KE, Jang KI, Kim J, Fu H, Huang X, Chava P, Wang R, Bhole S, Wang L, Na YJ, Guan Y, Flavin M, Han Z, Huang Y, Rogers JA. Soft microfluidic assemblies of sensors, circuits, and radios for the skin. Science. 2014; 344:70. [PubMed: 24700852]
32. Yeo JC, Yu J, Koh ZM, Wang Z, Lim CT. Wearable tactile sensor based on flexible microfluidics. Lab Chip. 2016; 16:3244–3250. [PubMed: 27438370]
33. Tekin E, Smith PJ, Schubert US. Inkjet printing as a deposition and patterning tool for polymers and inorganic particles. Soft Matter. 2008; 4:703–713.
34. Smith PJ, Shin DY, Stringer JE, Derby B, Reis N. Direct ink-jet printing and low temperature conversion of conductive silver patterns. J Mater Sci. 2006; 41:4153.
35. van den Berg AMJ, de Laat AWM, Smith PJ, Perelaer J, Schubert US. Geometric control of inkjet printed features using a gelating polymer. J Mater Chem. 2007; 17:677.
36. Joshipura ID, Ayers HR, Majidi C, Dickey MD. Methods to pattern liquid metals. J Mater Chem. 2015; 3:3834.

Highlights

- A unique method for fabricating microfluidic systems based on inkjet printing of Polyethylene glycol as a fugitive ink is introduced.
- The developed approach allows realizing microfluidic structures with controlled dimensions and high vertical resolution.
- The processing technique allows the realization of scalable and flexible microfluidic systems and microfluidic electronics.
- The developed technology allows fabricating microsystems with a range of structural and substrate material options.

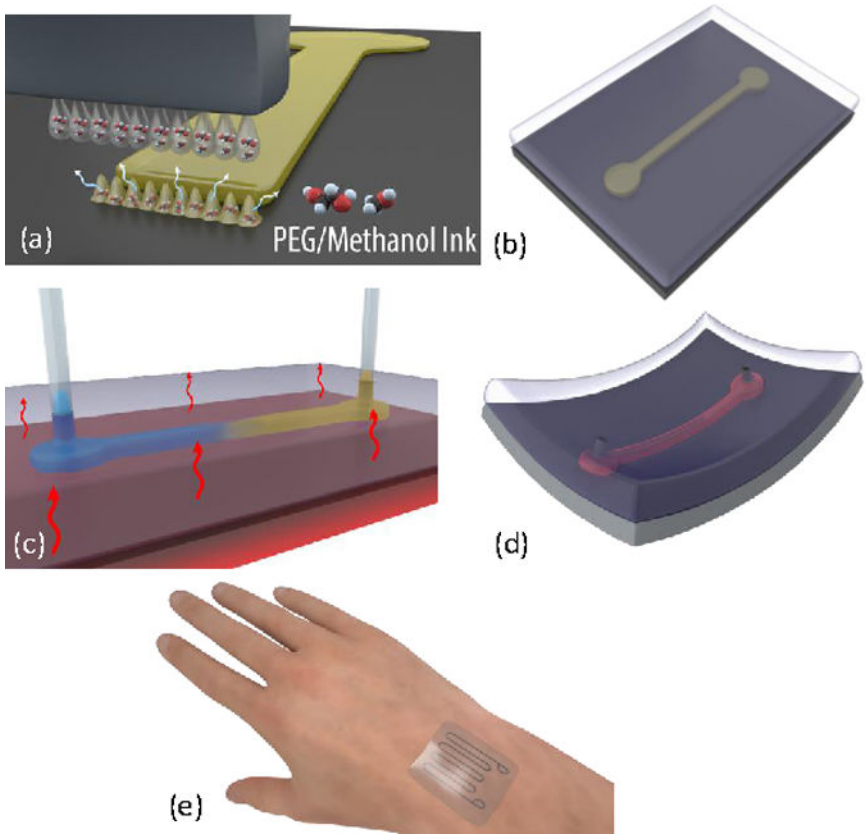

Fig. 1.

Illustration of the fabrication process. (a) Array of liquid PEG droplets are ejected from the inkjet printer and land on the target substrate to solidify and form the sacrificial layer of the microfluidic channel. (b) The structural layer is cast and cured to encapsulate the sacrificial layer. (c) Inlet and outlet ports are punched through the structural layer, PEG is heated above its phase change temperature, and IPA is injected from inlet to outlet to remove the PEG. (d) The flexible microfluidic channel is then filled with the target fluid. (e) Flexible and wearable liquid metal-based microfluidic strain sensor is an example application.

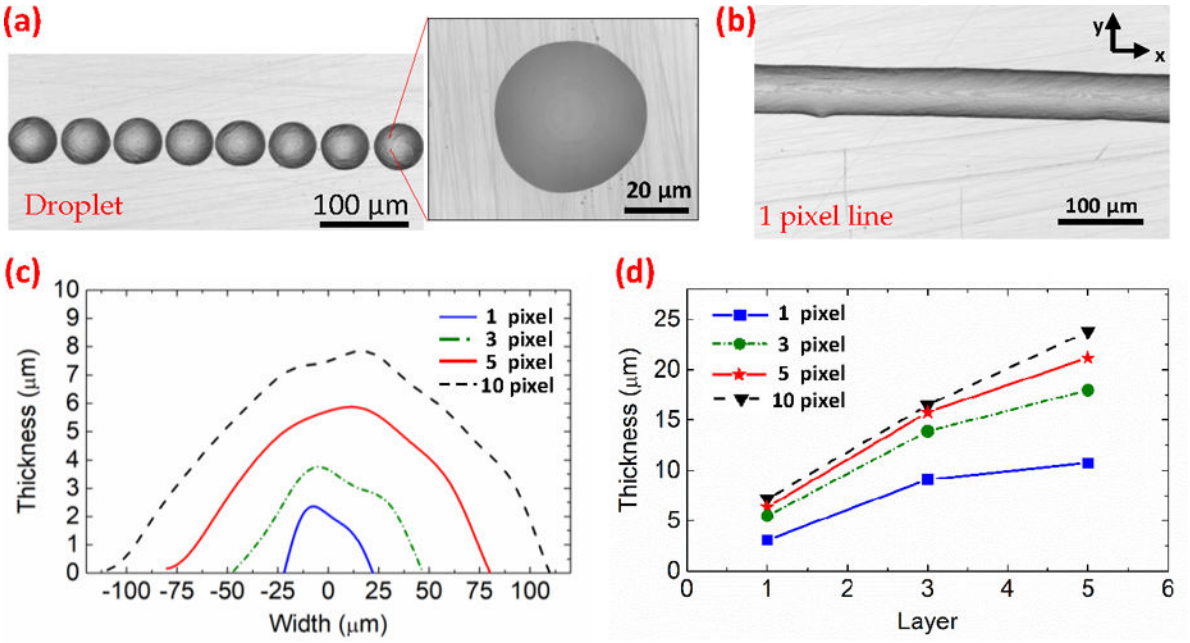

Fig. 2.

Performance of inkjet-printed PEG. (a) Optical microscope image of printed droplets at 90 µm spacing. (b) Microscope image of a single pixel line printed with 30 µm droplet spacing. (c) Printed lines with overlapping pixels showing the profile and the increase in width and thickness. (d) Printed film thickness scales linearly with the number of printed layers and increase with the number of pixels.

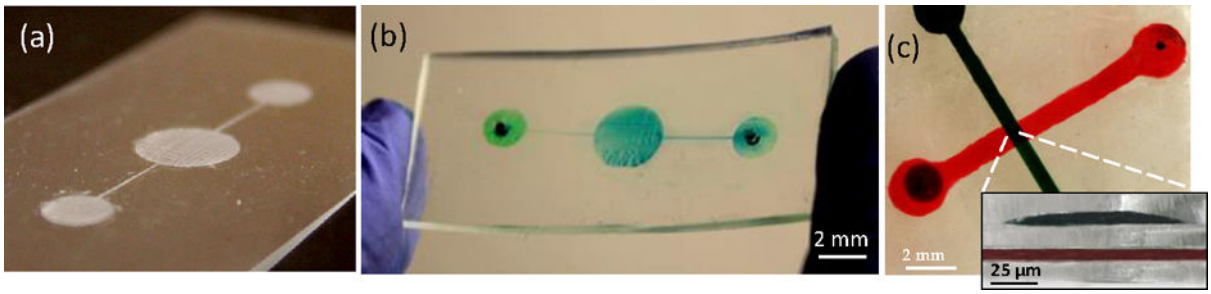

Fig. 3.

(a) Printed PEG sacrificial layer on PDMS substrate. (b) Microfluidic channel filled with a colored dye after encapsulating and dissolving the sacrificial layer shown in (a). (c) Multilayer microfluidic channels fabricated by printing two sacrificial layers with a structural layer realized in between. Inset shows the channel cross-section with the separation layer in between.

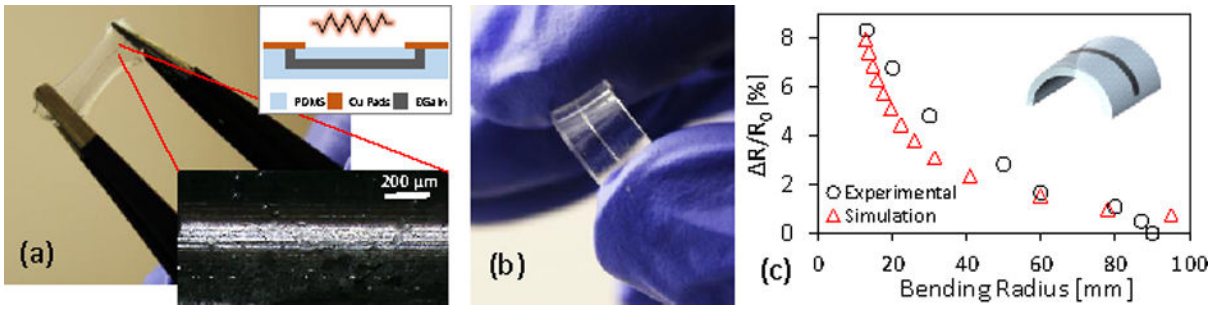

Fig. 4.

(a) Fabricated EGaIn flexible and strechable microfluidic resistor. Inset shows continous conductive path while stretching. (b) The resistor is flexible with geometric changes driving resistive sensor shifts. (c) Measured change in resisance at different bending radii are comparable to simulated results.

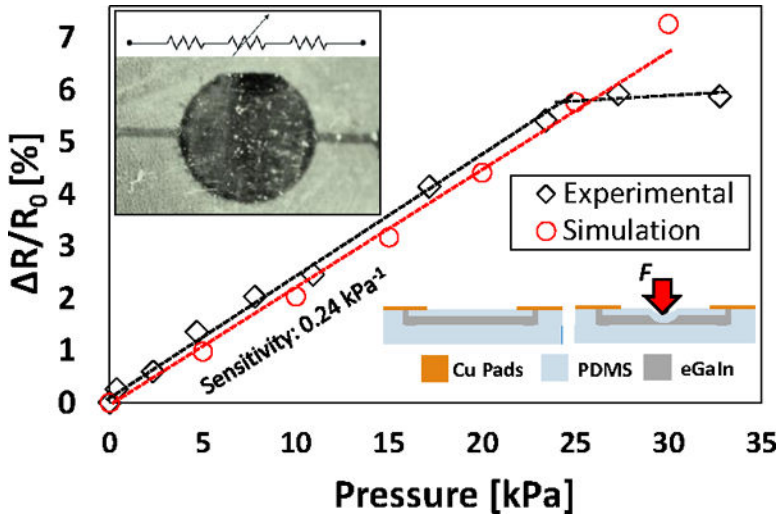

Fig. 5.

Experimental and simulated pressure response for the microfluidic pressure sensor. Linear operating range is shown with a stauration region beyond 25 kPa for the experimental results. Inset: a microscope image of the fabricated sensor with its working principle.